

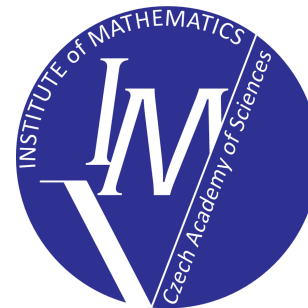
ON SOME COMPUTATIONAL CHALLENGES IN NUMERICAL SIMULATIONS OF STABLY STRATIFIED FLOWS

Tomáš Bodnár

December 7, 2021



Czech Technical University
Prague - Czech Republic



Institute of Mathematics
Czech Academy of Sciences

1. Mathematical Model

The full incompressible, viscous (laminar), variable density model can be written as:

$$\frac{\partial \rho}{\partial t} + \mathbf{u} \cdot \text{grad } \rho = 0 \quad , \quad (1)$$

$$\rho \left(\frac{\partial \mathbf{u}}{\partial t} + \text{div}(\mathbf{u} \otimes \mathbf{u}) \right) = -\text{grad } p + \text{div } 2\mu \mathbf{D} + \rho \mathbf{g} \quad . \quad (2)$$

These equations together with the incompressibility constraint $\text{div} \mathbf{u} = 0$ lead to the set of governing equations for the velocity $\mathbf{u}(\mathbf{x}, t)$, density $\rho(\mathbf{x}, t)$ and pressure field $p(\mathbf{x}, t)$.

This model is sometimes called the *non-homogeneous Navier-Stokes equations*, see e.g. *Lions* [16].

The pressure and density fields can be assumed to be a perturbation of the hydrostatic equilibrium state:

$$\begin{aligned} \rho(\mathbf{x}, t) &= \rho_0(\mathbf{x}) + \rho'(\mathbf{x}, t) & \text{i.e.} & \quad \rho(x, y, z, t) = \rho_0(z) + \rho'(x, y, z, t) \\ p(\mathbf{x}, t) &= p_0(\mathbf{x}) + p'(\mathbf{x}, t) & \text{i.e.} & \quad p(x, y, z, t) = p_0(z) + p'(x, y, z, t) \end{aligned}$$

The background density and pressure fields are linked by the hydrostatic relation:

$$\text{grad } p_0 = \rho_0 \mathbf{g} \quad \text{i.e.} \quad \frac{\partial p_0}{\partial z} = \rho_0 g \quad \text{where} \quad \mathbf{g} = (0, 0, g),$$

This leads to a rearranged momentum equations:

$$\rho \left(\frac{\partial \mathbf{u}}{\partial t} + \text{div}(\mathbf{u} \otimes \mathbf{u}) \right) = -\text{grad } p' + \text{div } 2\mu \mathbf{D} + \underbrace{(\rho - \rho_0)}_{\rho'} \mathbf{g} \quad .$$

So far **no approximations** were made.

The *Boussinesq approximation* is obtained from the full model by replacing the complete density $\rho(\mathbf{x}, t)$ on the left hand side of momentum equation by a suitable fixed (in space and time) characteristic density ρ^* .

$$\begin{aligned} \frac{\partial \rho}{\partial t} + \mathbf{u} \cdot \text{grad } \rho &= 0 \\ \rho^* \left(\frac{\partial \mathbf{u}}{\partial t} + \text{div}(\mathbf{u} \otimes \mathbf{u}) \right) &= -\text{grad } p' + \text{div } 2\mu \mathbf{D} + (\rho - \rho_0) \mathbf{g} \quad . \end{aligned}$$

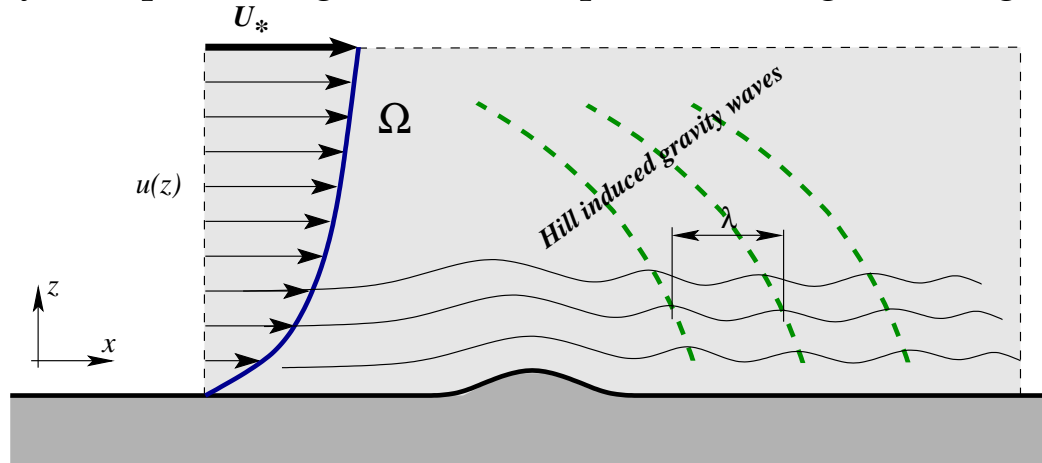
This system was used in the numerical simulations presented hereafter.

It is often equivalently rewritten in terms of the density perturbation as:

$$\begin{aligned} \frac{\partial \rho'}{\partial t} + \mathbf{u} \cdot \text{grad } \rho' &= -w\gamma \quad \text{where} \quad \gamma = \frac{\partial \rho_0}{\partial z} \\ \rho^* \left(\frac{\partial \mathbf{u}}{\partial t} + (\mathbf{u} \cdot \text{grad}) \mathbf{u} \right) &= -\text{grad } p' + \text{div } 2\mu \mathbf{D} + \rho' \mathbf{g} \quad . \end{aligned}$$

2. Stably Stratified Flows - basic phenomena

The stable density/temperature gradient is responsible for generating waves in the flow field.



These waves are characterized by the Brunt–Väisälä frequency

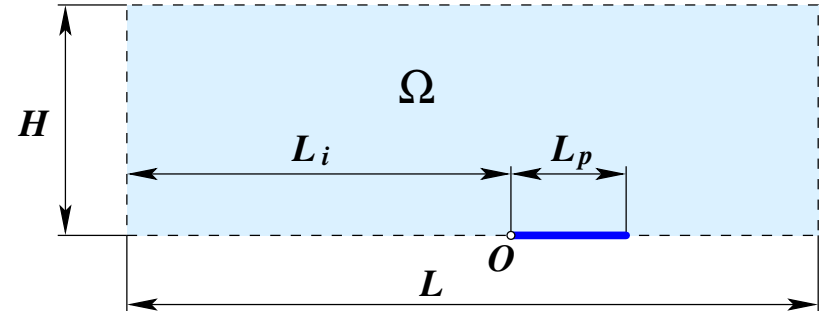
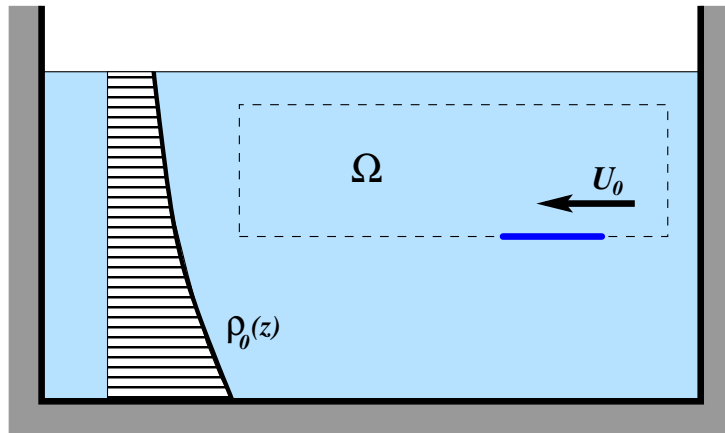
$$N = \sqrt{\frac{g}{\rho^*} \frac{\partial \rho_0}{\partial z}} = \sqrt{-\frac{g}{\Theta^*} \frac{\partial \Theta_0}{\partial z}} \quad (3)$$

The wavelength can be estimated as $\lambda \approx U^*/N$.

Flow over horizontal strip

Test case configuration

The 2D computational domain represents a rectangle attached to a horizontal plate moving in a towing tank (the physical domain). *Chashechkin & Mitkin [6], Chashechkin, Mitkin, & Bardakov [7]*



The dimensions are set to $L = 1.5 \text{ m}$, $H = 0.5 \text{ m}$, $L_i = 1.0 \text{ m}$, $L_p = 0.025 \text{ m}$. The grid has 258×117 points with the minimum cell size in the near-wall region $\Delta z = 0.5 \text{ mm}$

Boundary conditions

Two-dimensional case is considered and thus only boundary conditions are given for this 2D case (in x - z coordinates only).

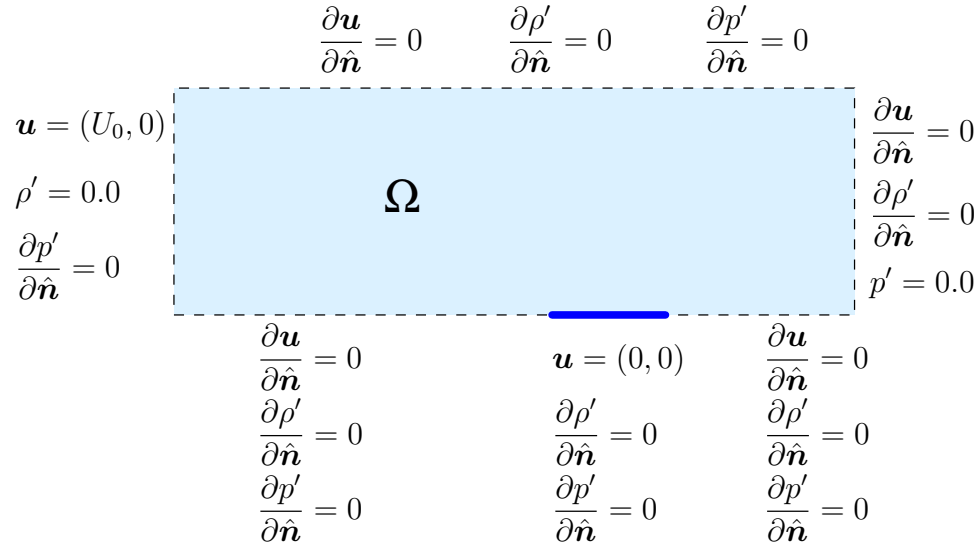
- **Inlet** ... The constant velocity profile $\mathbf{u} = (U_0, 0)$ is prescribed. The horizontal velocity component u is equal to $U_0 = 0.17\text{cm/s}$ or $U_0 = 0.25\text{cm/s}$. Density perturbation ρ' is set to zero, while homogeneous Neumann condition is used for pressure.
- **Free stream - Upper boundary** ... Homogeneous Neumann condition is used for velocity components and density perturbations. Pressure is prescribed as a constant along the outlet boundary.

The background density field is given by

$$\rho_0(z) = \rho_* \exp\left(-\frac{z}{\Lambda}\right) \quad \text{with} \quad \rho_* = 1000 \text{ kg} \cdot \text{m}^{-3} \quad \text{and} \quad \Lambda = 50\text{m} \quad .$$

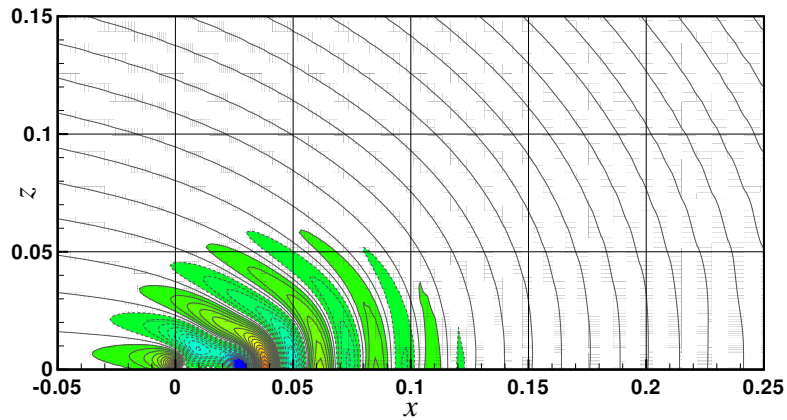
The other parameters are dynamical viscosity $\mu = 10.0^{-3} \text{ kg} \cdot \text{m}^{-1} \cdot \text{s}^{-1}$ and gravity acceleration $g = -10.0 \text{ m} \cdot \text{s}^{-2}$.

Boundary conditions summary

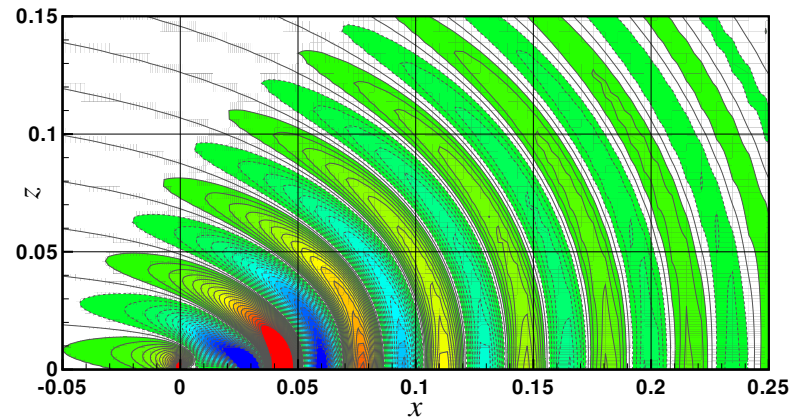


Numerical Results

Vertical velocity contours

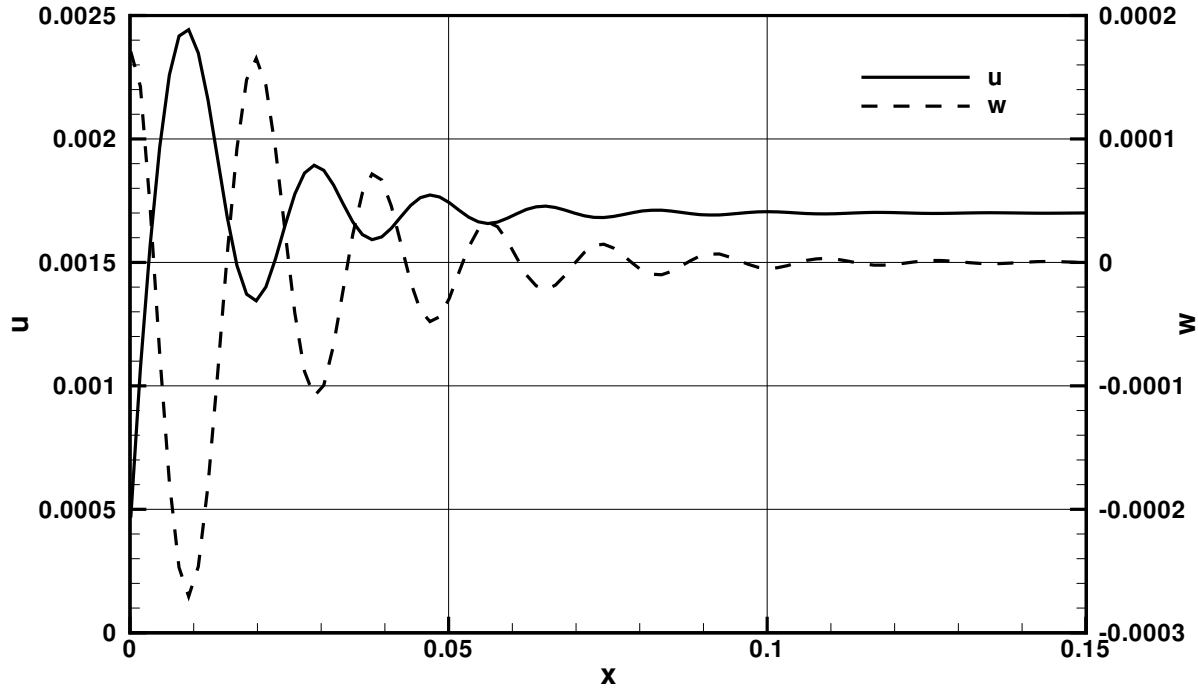


$$U_0 = 0.17 \text{ cm/s}$$



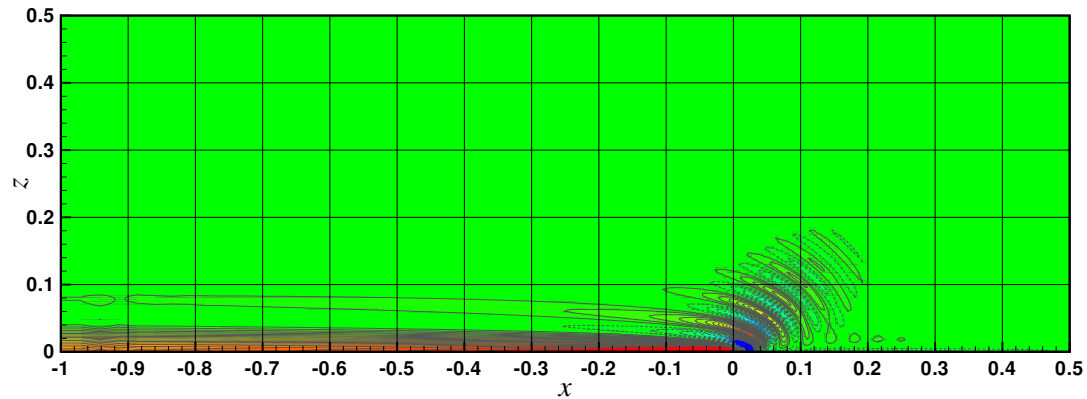
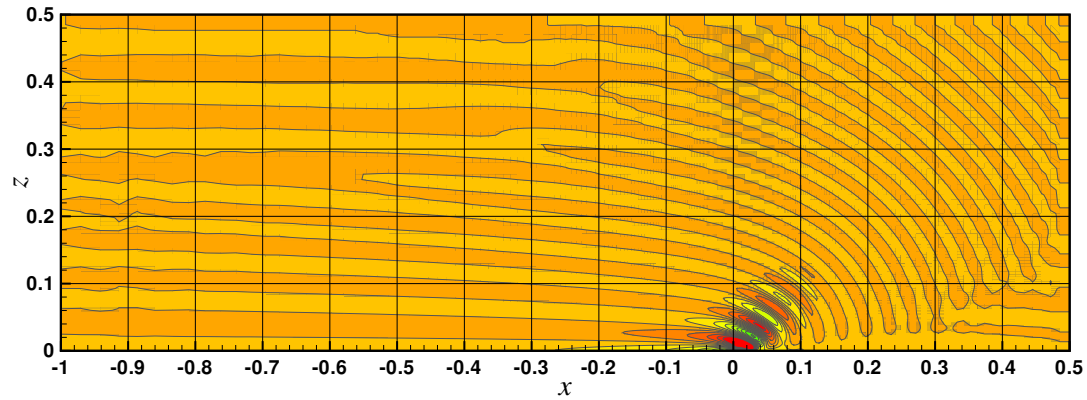
$$U_0 = 0.25 \text{ cm/s}$$

Velocity profiles



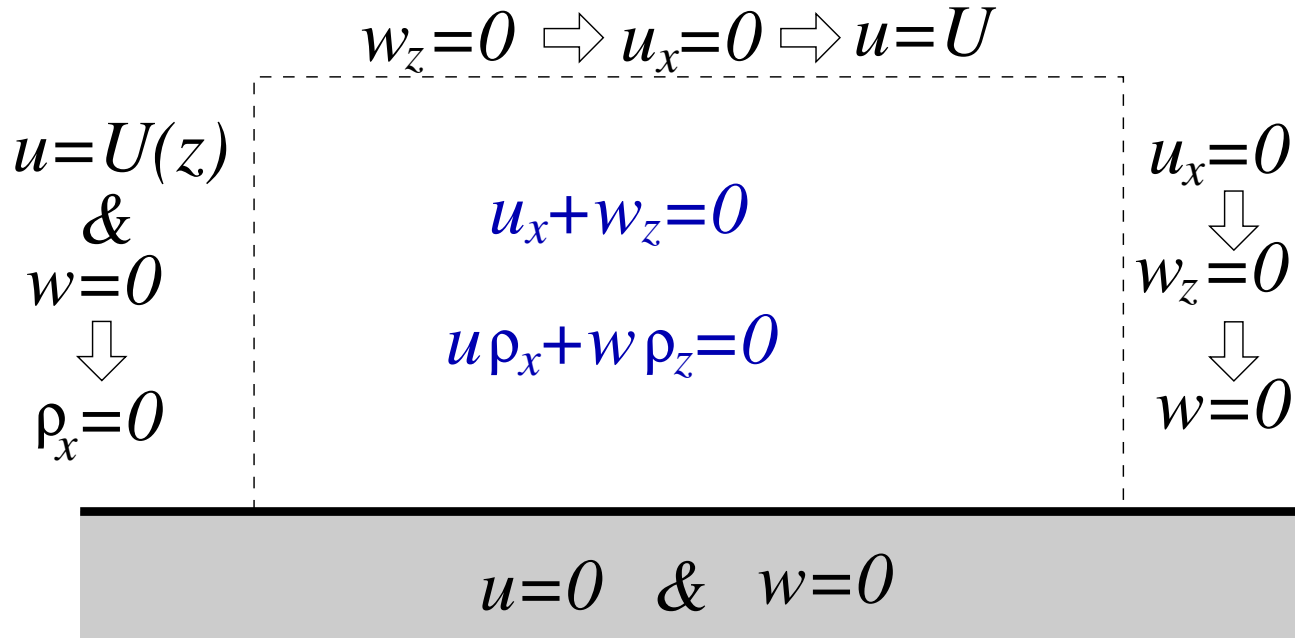
Cut taken from the strip leading edge at the angle of 45 degrees ($U_0 = 0.17\text{cm/s}$).

Global view - Whole domain



Horizontal velocity and pressure contours ($U_0 = 0.25\text{cm/s}$).

First Problems - Compatibility of boundary conditions



- “soft” conditions are not soft enough
- velocity and density conditions are strongly coupled
- unfortunately $\rho_x = 0$ at the inlet is not a good choice

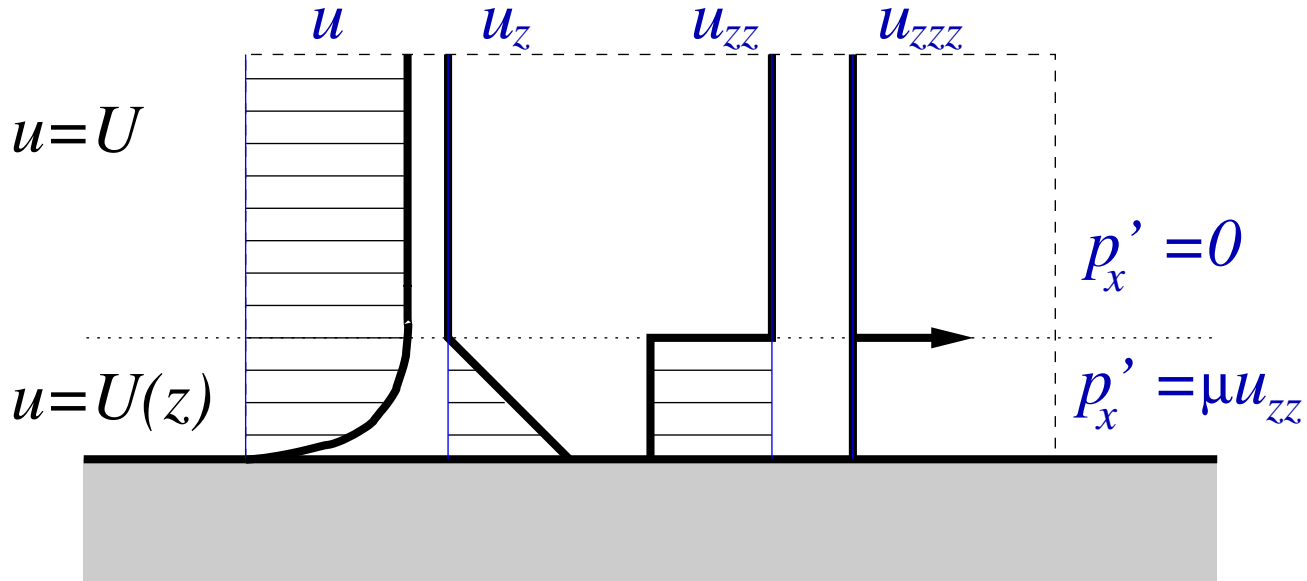
$$\begin{aligned}\rho^*(u_t + uu_x + wu_z) &= -p'_x + \mu(u_{xx} + u_{zz}) \\ \rho^*(w_t + uw_x + ww_z) &= -p'_z + \mu(w_{xx} + w_{zz}) + g\rho'\end{aligned}$$

$$\begin{array}{l} u = U(z) \\ \& \\ w = 0 \\ \Downarrow \\ \rho_x = 0 \end{array} \Rightarrow \rho'_x = 0 \quad ! \quad \begin{array}{l} p'_x = \mu u_{zz} \\ p'_z = g\rho' \\ \Downarrow \\ \rho'_x = \frac{\mu}{g} u_{zzz} \end{array}$$

$$\bullet \rho'_x \propto u_{zzz} \quad \Longrightarrow \quad u\rho'_x + w\rho'_z = -\gamma w$$

- inlet velocity profile generates vertical velocity perturbation

Suitable velocity profiles?



- not every velocity profile can guarantee a fully developed density profile

- $\rho'_x = 0 \iff u_{zzz} = 0$

- $U(z) = a_0 + a_1 z + a_2 z^2$ where $a_0 = 0$ for no-slip condition

3. Numerical Methods in Detail

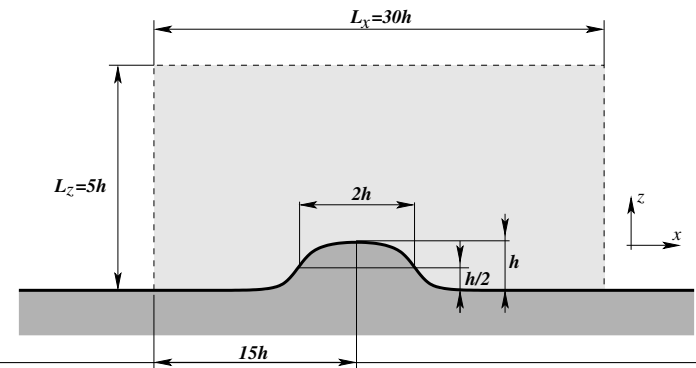
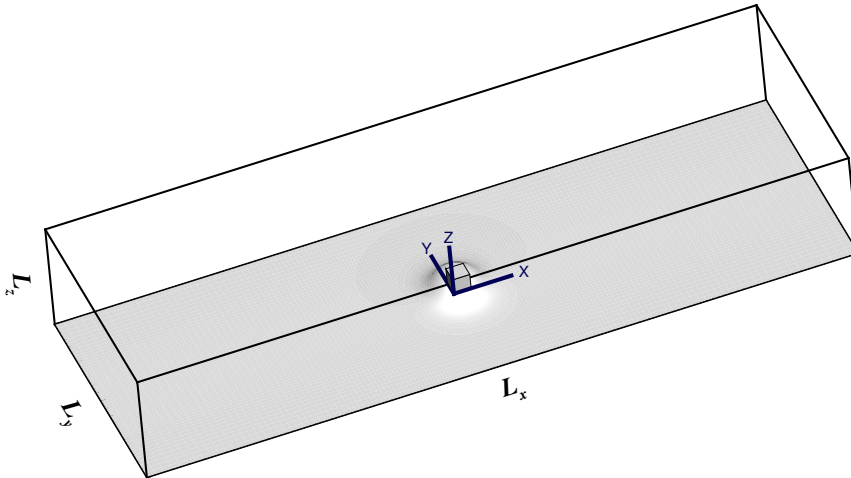
- **Time-marching method** – The steady solution is reached as a limit for $t \rightarrow \infty$
- **Artificial compressibility** – A pseudo-time derivative of pressure is added to the continuity equation (i.e. the divergence-free constraint) to enforce the incompressibility.
- **Semi-discretization (method of lines)** – The system of PDE's is first discretized in space, which leads to a system of ODE's describing the temporal evolution at every grid point.
- **Compact finite-difference space discretization** – High-resolution approximation of spatial derivatives, using rather compact computational stencil.
- **SSP Runge-Kutta time stepping** – A time-integration method that doesn't introduce non-physical oscillations to the numerical solution.
- **Low-pass filter stabilization** – Compact filters are used to remove high- (i.e. grid-) frequency oscillations from numerical solution, while the longer wavelengths remain undamped.

4. Flow Over a Hill - Computational Setup

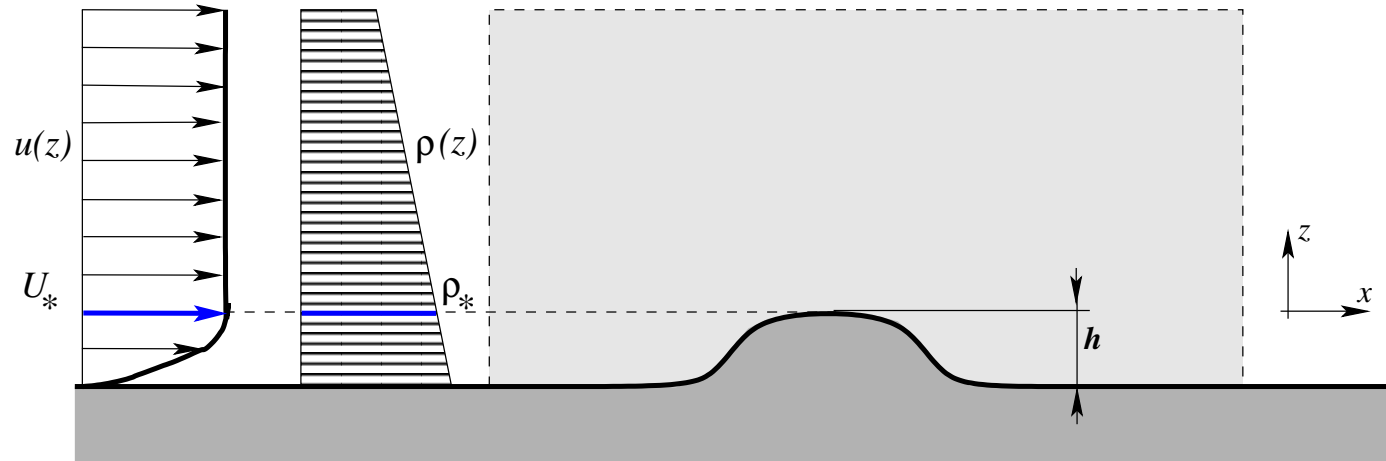
The hill shape is the same as in *Hunt & Snyder* [14], resp. *Ding, Calhoun, & Street* [8], i.e. the surface elevation $z_s(r)$ is given by an inverse of a fourth order polynomial in terms of a distance r from the hill symmetry axis.

$$z_s(r) = \frac{h}{1 + (r/h)^4}$$

The domain dimensions are $L_x = 30h$, $L_y = 10h$, $L_z = 5h$.



Physical parameters



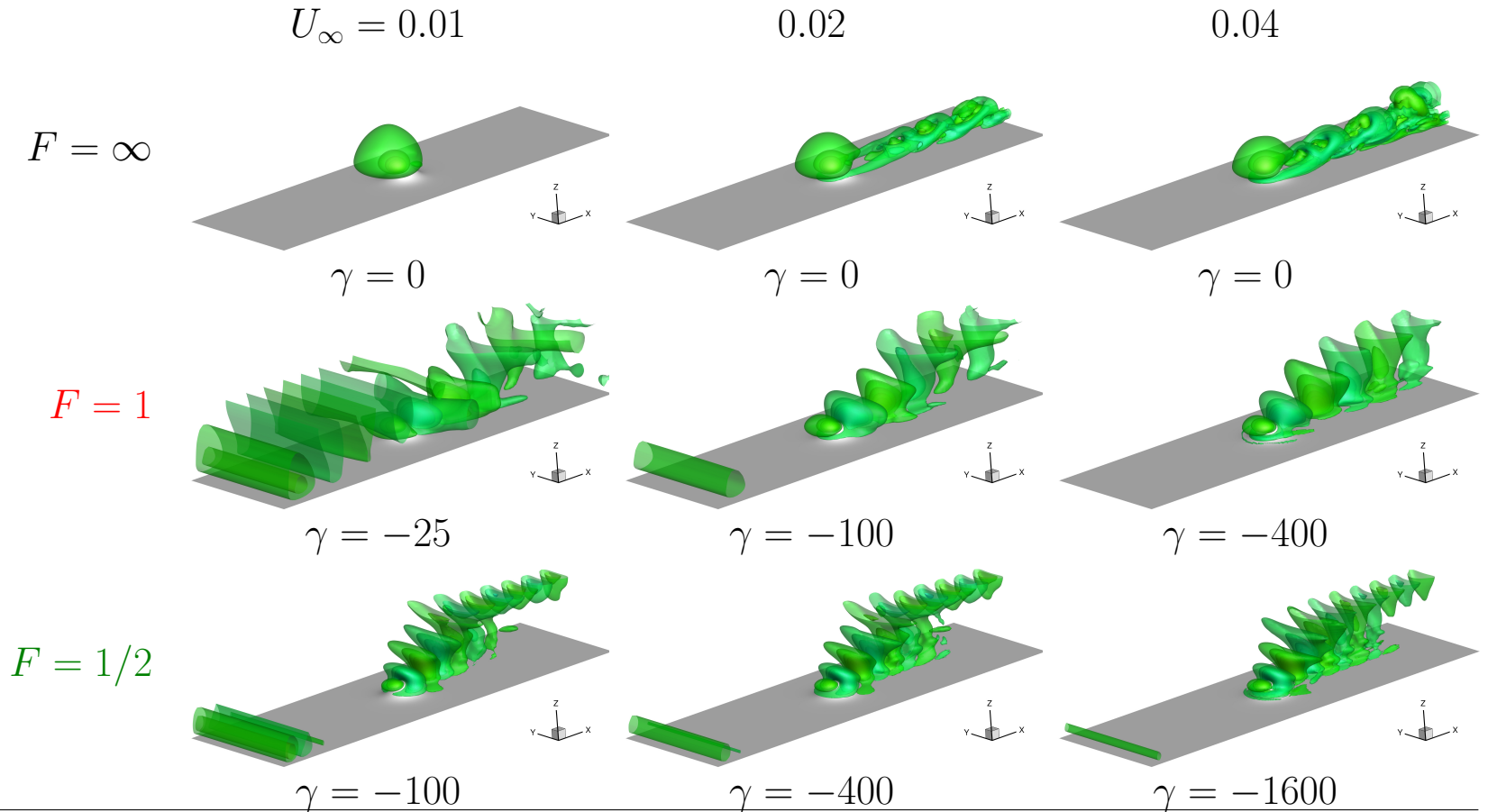
The fluid is characterized by density $\rho^* = 1000 \text{ kg} \cdot \text{m}^{-3}$ and dynamical viscosity $\mu = 10^{-3} \text{ kg} \cdot \text{m}^{-1} \cdot \text{s}^{-1}$. The **linear background density profile** is defined by $\rho_0(z) = \rho^* + \gamma \cdot (z - h)$. The gravity acceleration acts against the z coordinate, so $g = -10 \text{ m} \cdot \text{s}^{-2}$. The hill height $h = 2 \text{ cm} = 0.02 \text{ m}$ was chosen as the characteristic length scale for both, the Reynolds number (where h represents the boundary layer thickness) as well as for the Froude number (where h represents the vertical displacement scale).

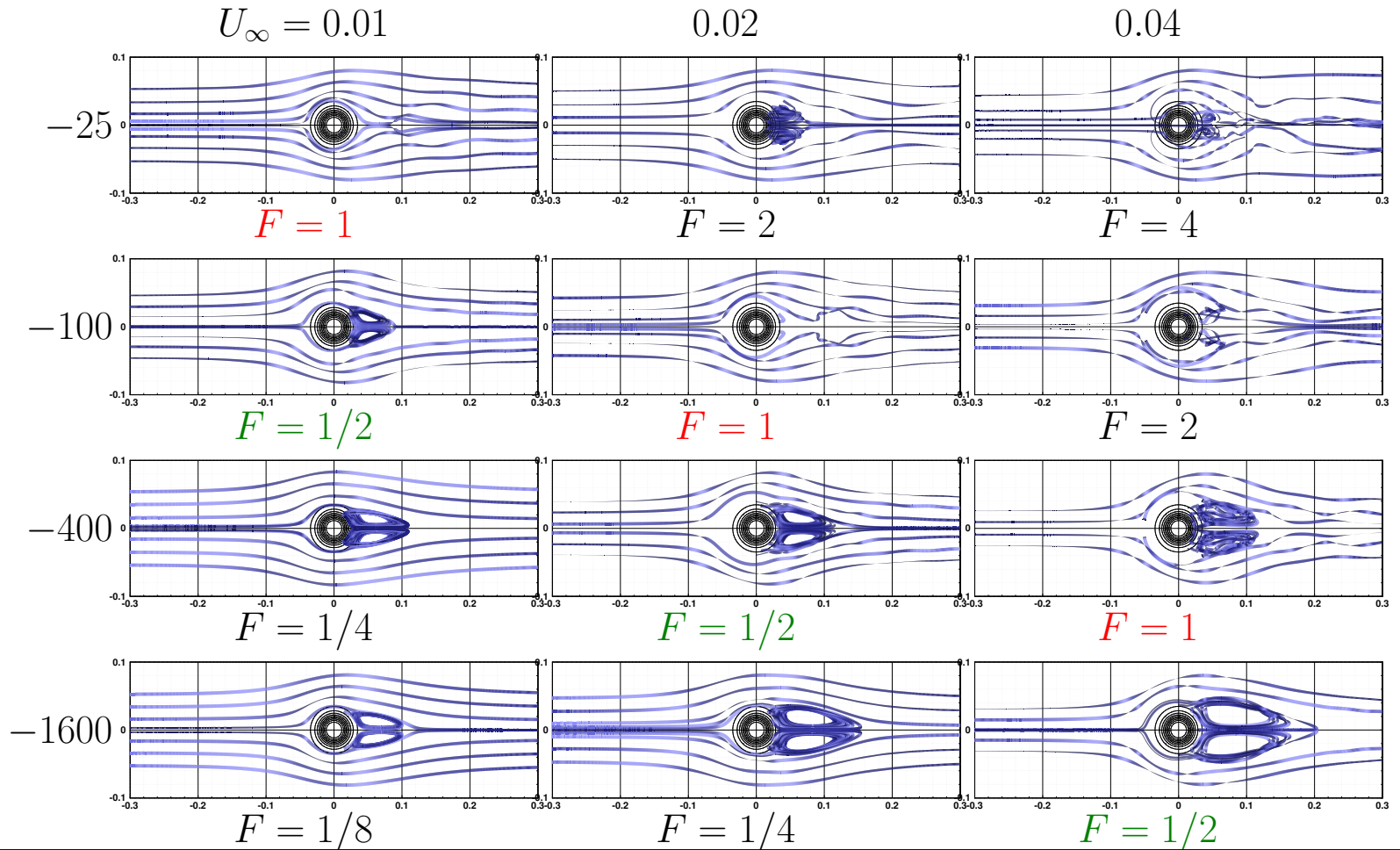
The two physical quantities that are being varied in simulations are the characteristic (free stream) velocity $U_\infty [m \cdot s^{-1}]$ and the background density gradient $\gamma = \frac{\partial \rho_0}{\partial z} [kg \cdot m^{-4}]$. The Froude number is then given by

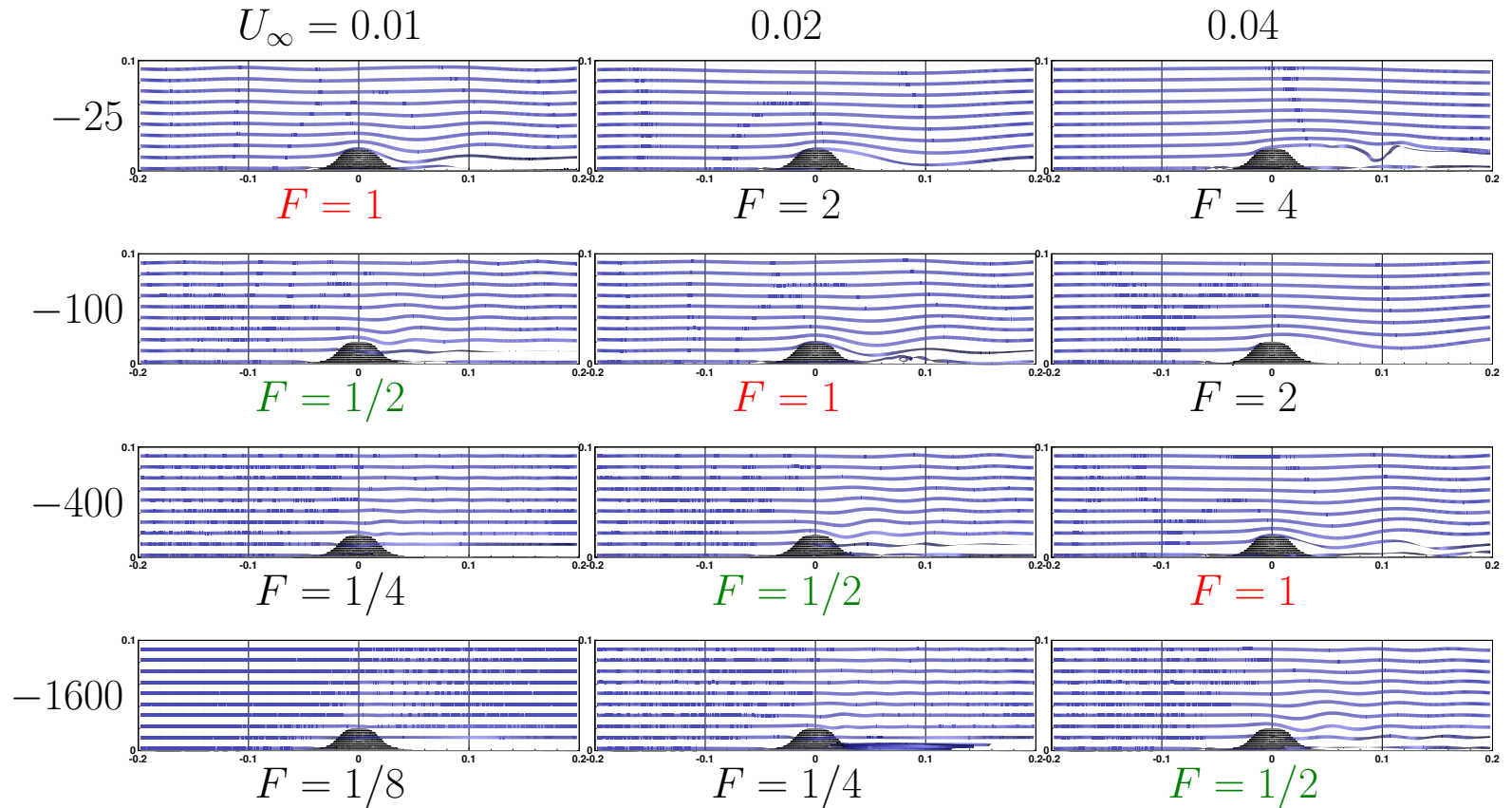
$$F = \frac{U_\infty}{Nh} = \frac{U_\infty}{0.1\sqrt{|\gamma|} \cdot 0.02} = 500 \frac{U_\infty}{\sqrt{|\gamma|}} = \frac{1}{400} \frac{Re}{N}$$

	$\gamma = 0$ $N = 0$	$\gamma = -25$ $N = 1/2$	$\gamma = -100$ $N = 1$	$\gamma = -400$ $N = 2$	$\gamma = -1600$ $N = 4$
$U_\infty = 0.01$ $Re = 200$	∞	1	1/2	1/4	1/8
$U_\infty = 0.02$ $Re = 400$	∞	2	1	1/2	1/4
$U_\infty = 0.04$ $Re = 800$	∞	4	2	1	1/2

5. Preliminary Simulations







Boundary issues

- Sensitivity to boundary conditions
- Non-physical effects due to boundary conditions
- Long-range influence of boundary conditions
- Coupling between boundary conditions
- Convergence issues
- Well posedness issues
- Physical / Mathematical / Numerical conditions

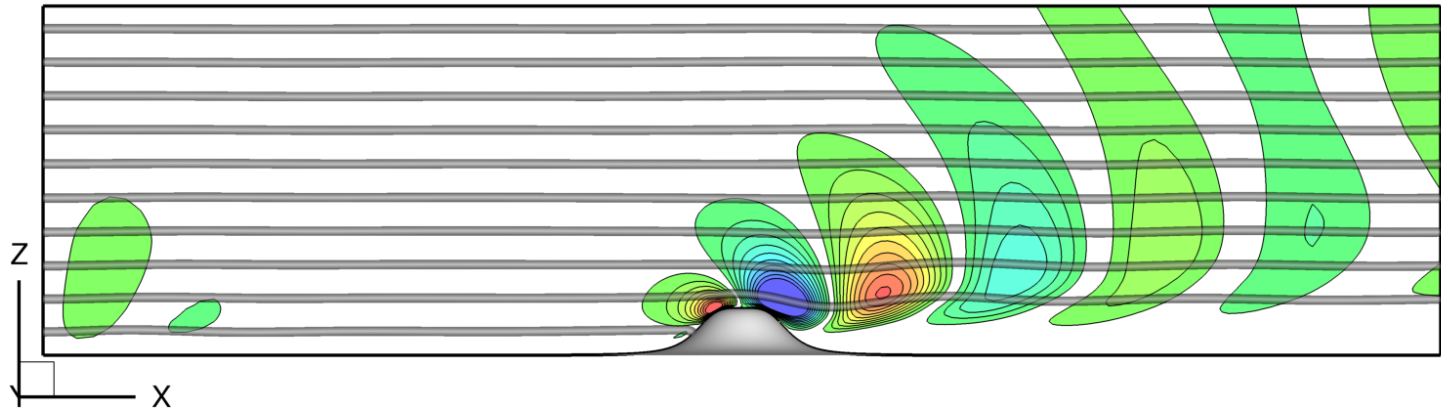
the end ...

6. Boundary Conditions

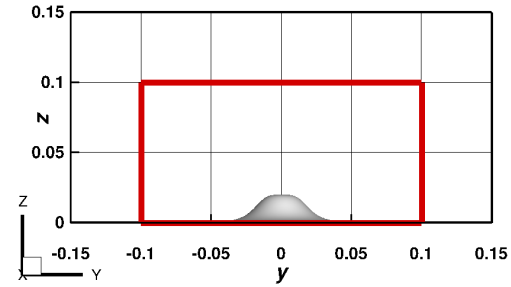
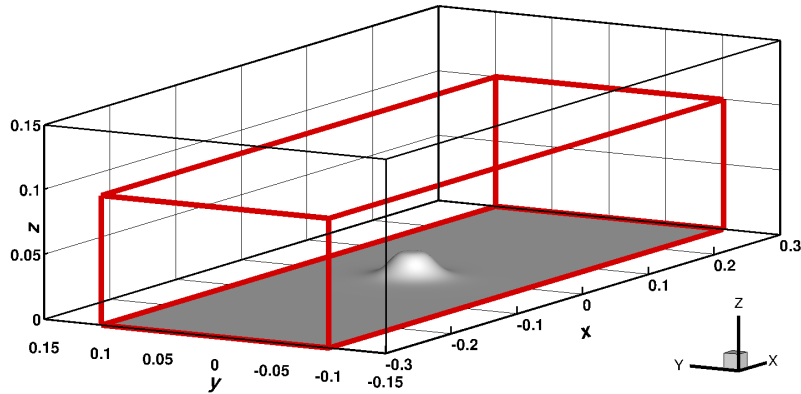
The standard computational setup used in the below discussed series of simulations is based on the following boundary conditions:

- **Inlet** ... The velocity profile $\mathbf{u} = (u(z), 0, 0)$ is prescribed. The horizontal velocity component u is given by the second order Pohlhausen-Kármán profile $u(z) = U_* (2\tilde{z} - \tilde{z}^2)$, where non-dimensional height \tilde{z} is defined using the boundary layer thickness $H = L_z$ as $\tilde{z} = z/H$. Density perturbation ρ' is set to zero, i.e. $\rho = \rho_0(z)$.
- **Outlet** ... All velocity components and also the density (perturbation) are extrapolated.
- **Wall** ... No-slip conditions are used on the wall, i.e. the velocity vector is set to $\mathbf{u} = (0, 0, 0)$. The density is extrapolated.
- **Free stream** ... All velocity components and also the density are extrapolated.
- **Sides** ... All velocity components and also the density are extrapolated.

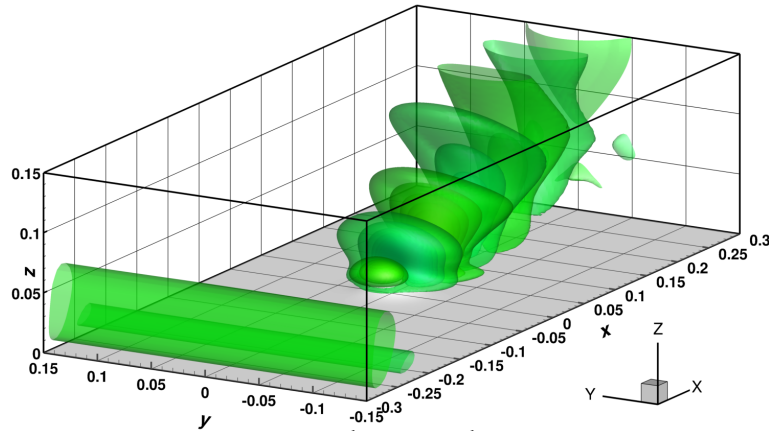
Vertical velocity contours and flow streamlines in the plane of symmetry.



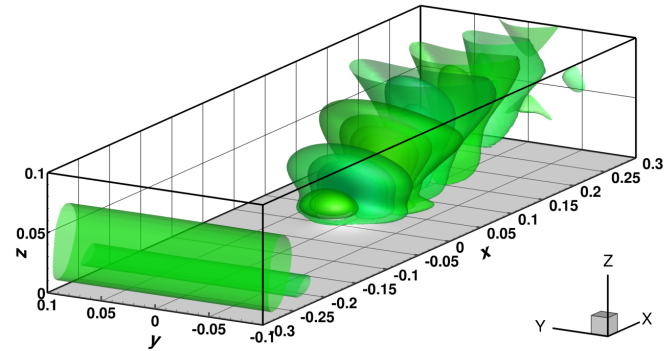
- Boundary is purely artificial
- Inlet/Outlet type is not a-priori defined
- Velocity vector is almost parallel to the boundary
- Far-field boundary is not “far enough”



Vertical velocity isosurfaces.

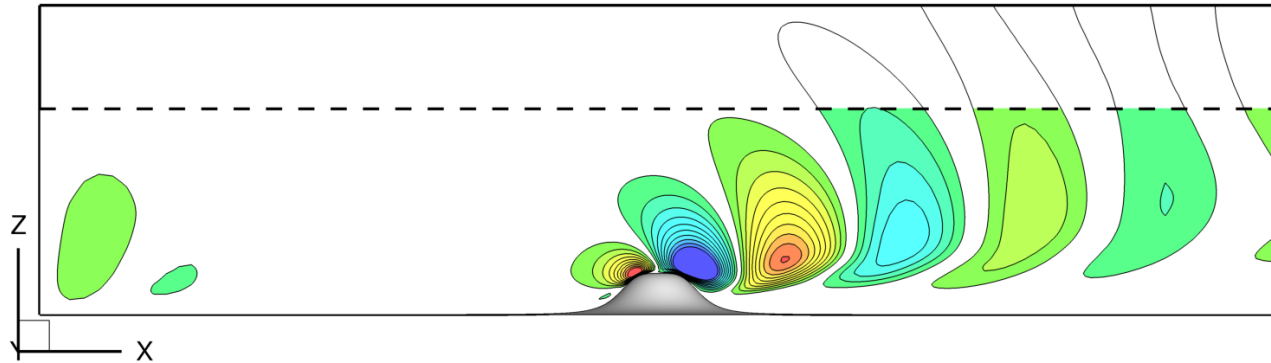


complete solution

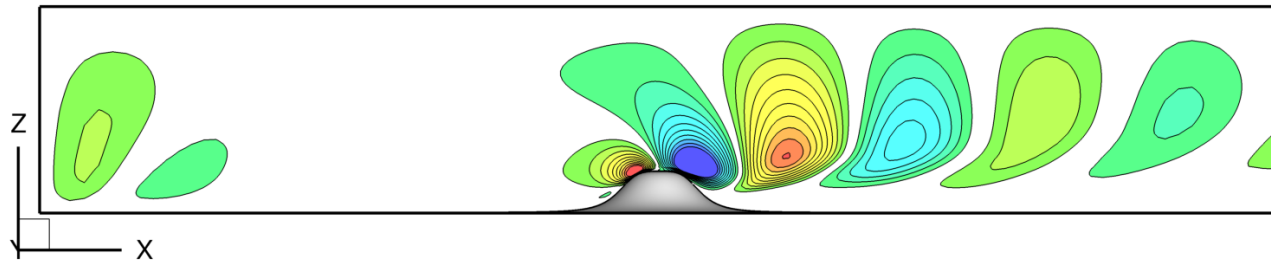


truncated solution

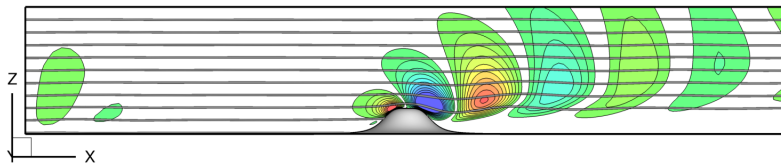
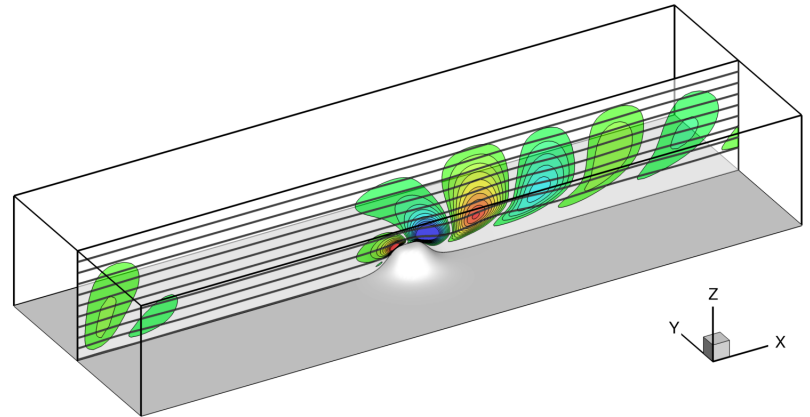
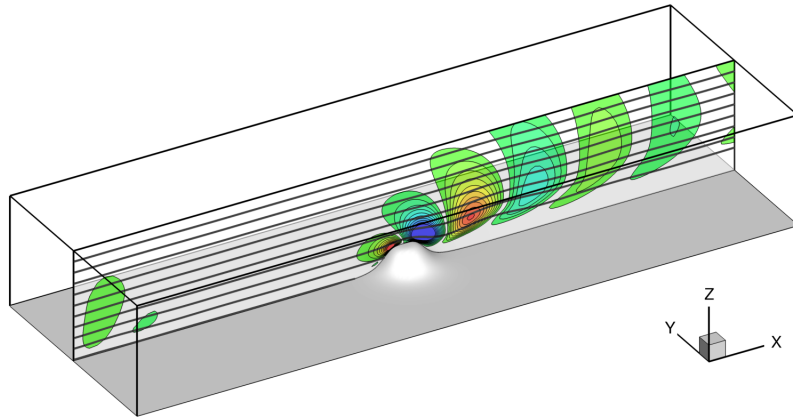
Vertical velocity contours in the plane of symmetry – truncated solution.



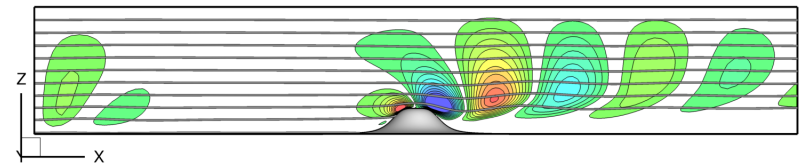
Vertical velocity contours in the plane of symmetry – truncated domain – $\frac{\partial p}{\partial n} = 0$.



Contours of the vertical velocity component w and flow streamlines.

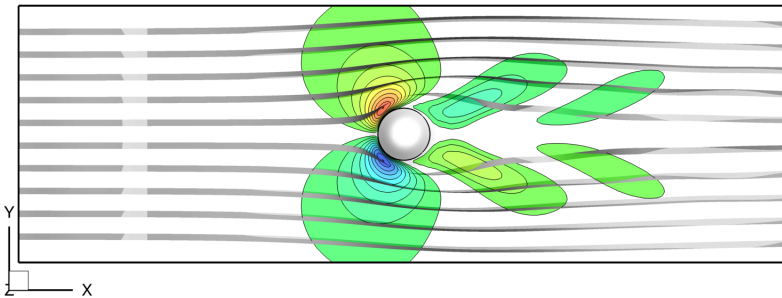
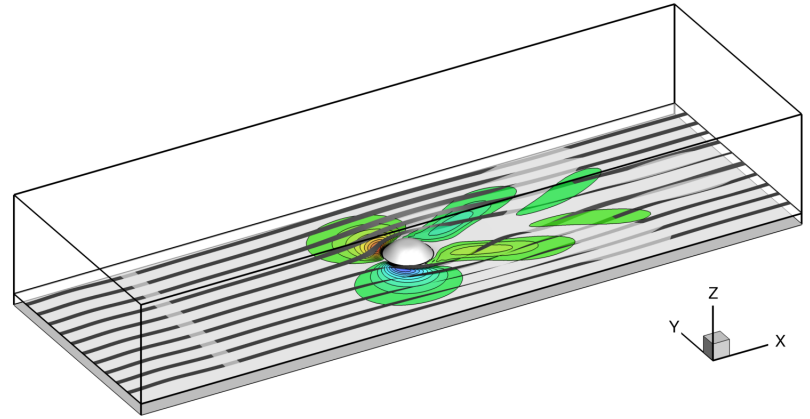
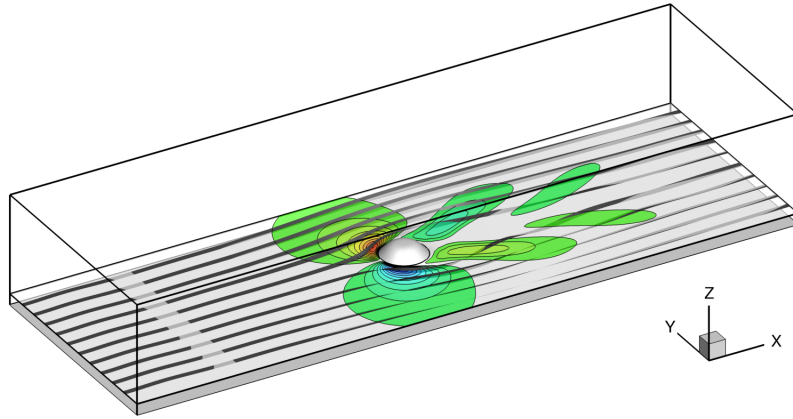


truncated solution

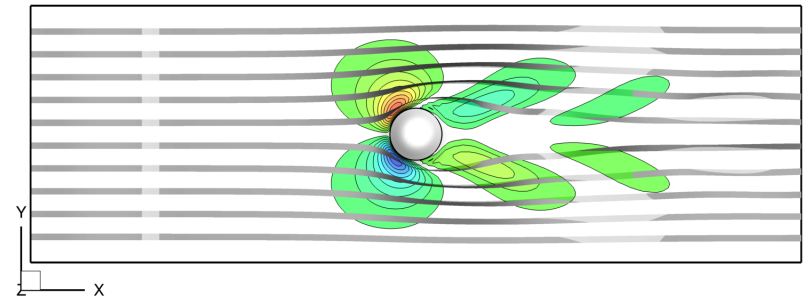


truncated domain - $\frac{\partial p}{\partial n} = 0$

Contours of the transversal velocity component v and flow streamlines.

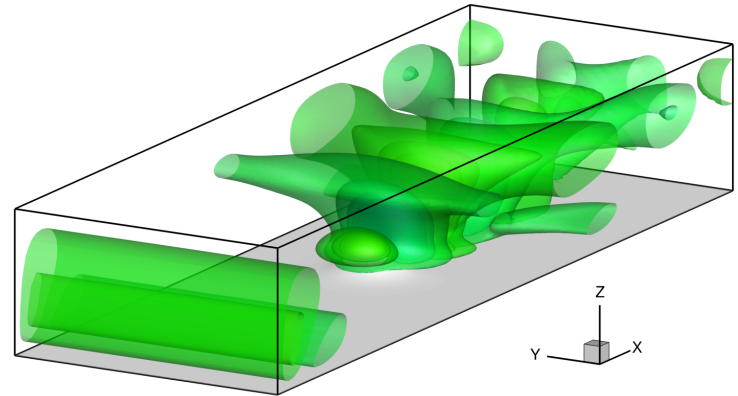
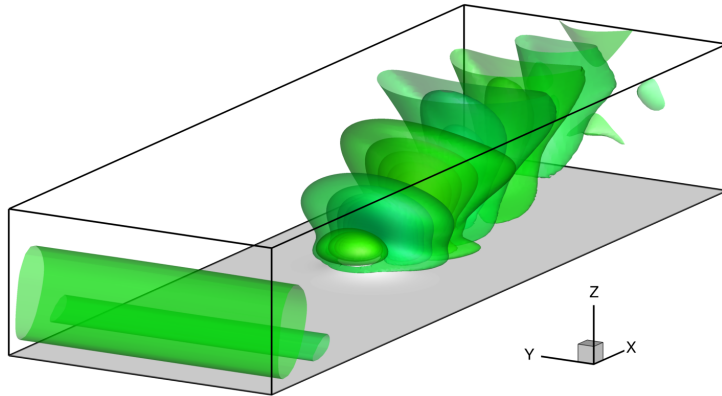


truncated solution

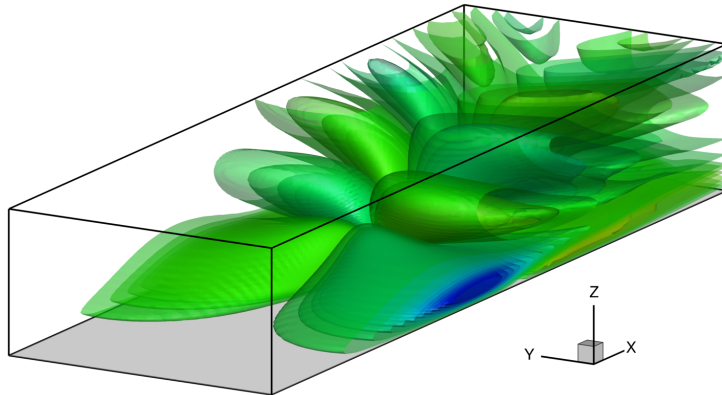


truncated domain $-\frac{\partial p}{\partial n} = 0$

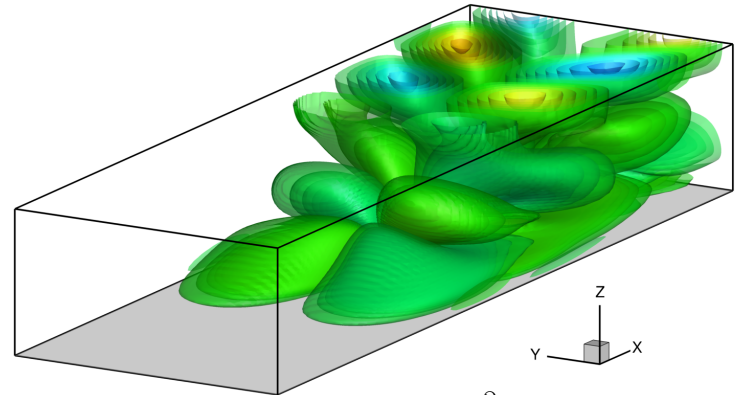
Isosurfaces of the vertical velocity component w .



Isosurfaces of the transversal velocity component v .



truncated solution



truncated domain – $\frac{\partial p}{\partial n} = 0$

Other (better) options?

- Do-Nothing condition (*Rannacher, Heywood, Turek (1993)*) [13]

$$p = \mu \frac{\partial u_n}{\partial n} \quad \text{and} \quad \mu \frac{\partial u_\tau}{\partial n} = 0$$

- Directional Do-Nothing condition (*Braack, Mucha (2014)*) [5]

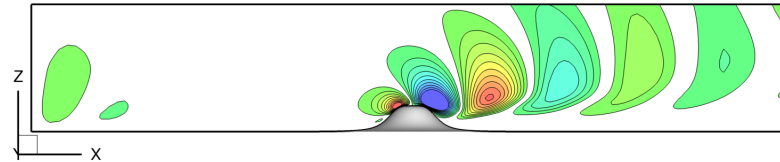
$$p = \mu \frac{\partial u_n}{\partial n} - \frac{1}{2} \rho u_n^- u_n$$

- “Do-Something” condition – *Convective Pressure Derivative (CPD)* [4, 3]

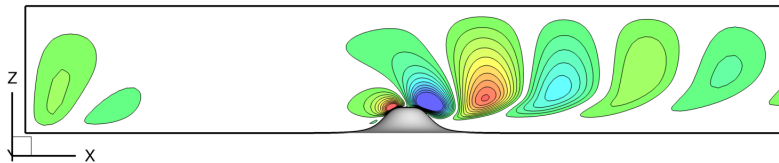
$$\frac{\partial p}{\partial n} = \rho^* |\mathbf{u}| \frac{\partial u_n}{\partial n}$$

7. Numerical Results

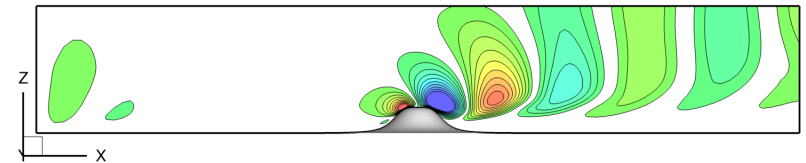
Contours of the vertical velocity component w - nondimensionalized $\tilde{w} = w/U_*$.



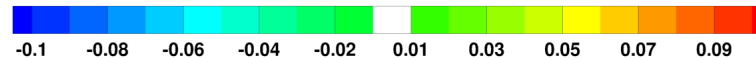
truncated solution



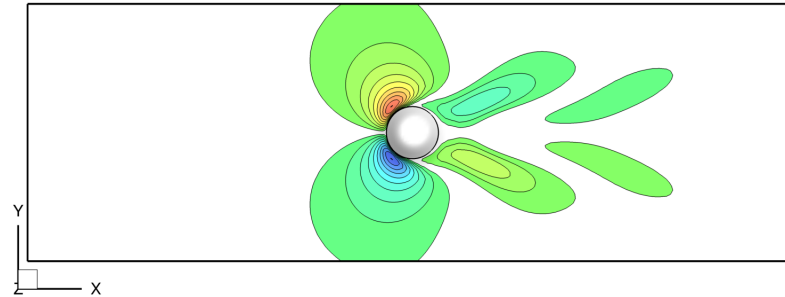
truncated domain - $\frac{\partial p}{\partial n} = 0$



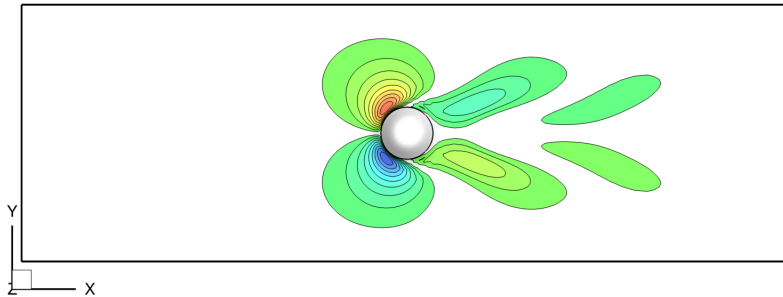
truncated domain - CPD



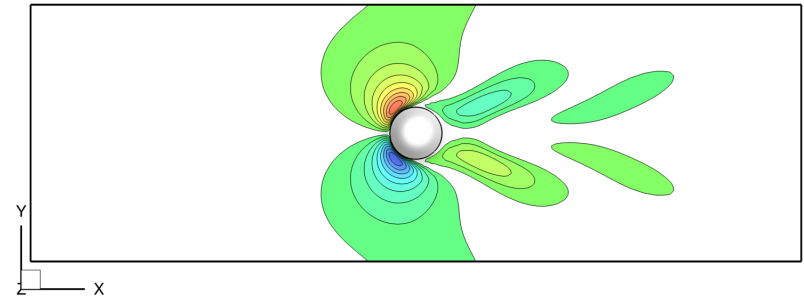
Contours of the transversal velocity component v - nondimensionalized $\tilde{v} = v/U_*$.



truncated solution



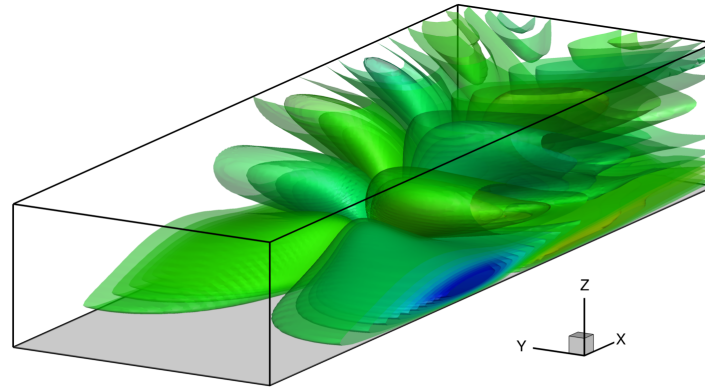
truncated domain - $\frac{\partial p}{\partial n} = 0$



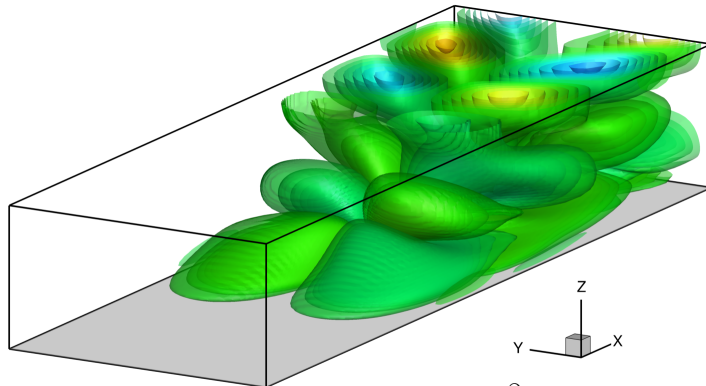
truncated domain - CPD



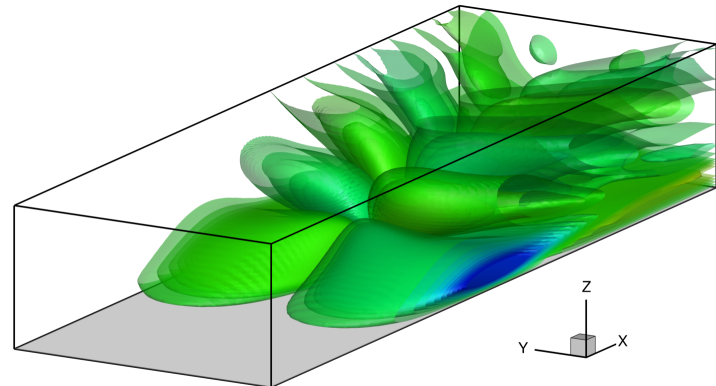
Isosurfaces of the transversal velocity component v - nondimensionalized $\tilde{v} = v/U_*$.



truncated solution



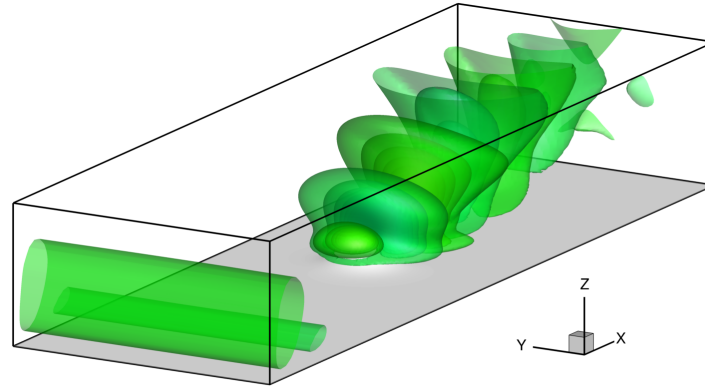
truncated domain - $\frac{\partial p}{\partial n} = 0$



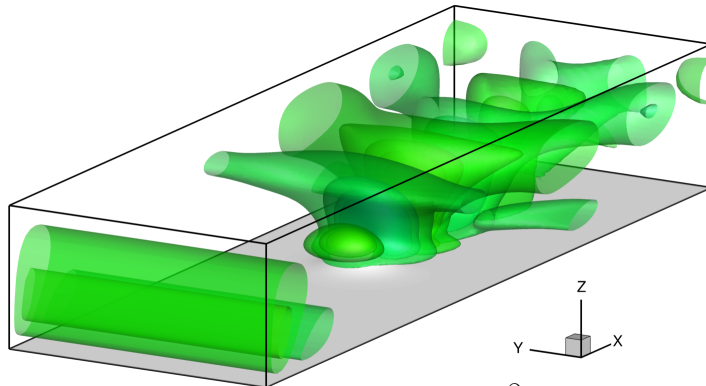
truncated domain - CPD



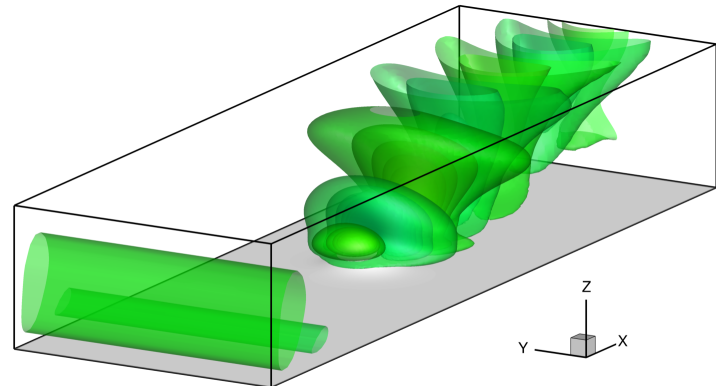
Isosurfaces of the vertical velocity component w - nondimensionalized $\tilde{w} = w/U_*$.



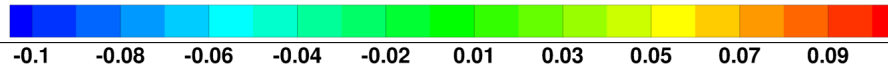
truncated solution



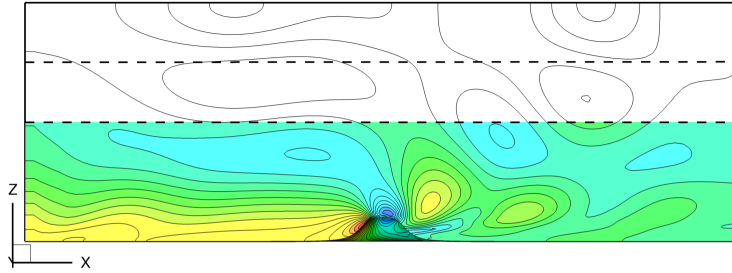
truncated domain - $\frac{\partial p}{\partial n} = 0$



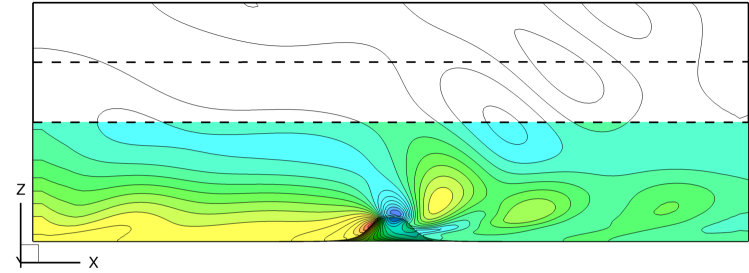
truncated domain - CPD



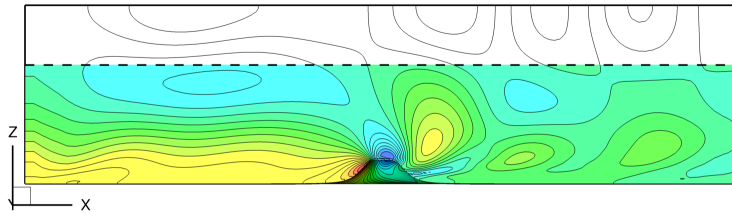
Pressure contours in the plane of symmetry.



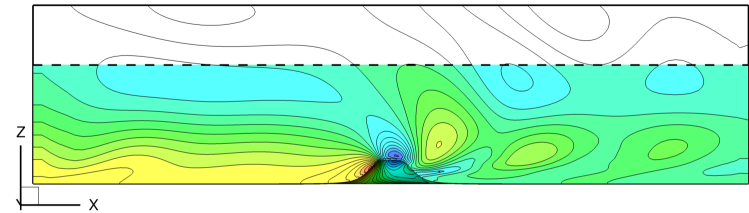
truncated domain +2H



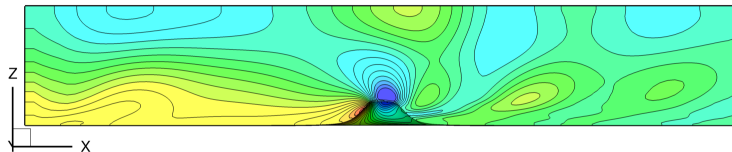
truncated domain +2H



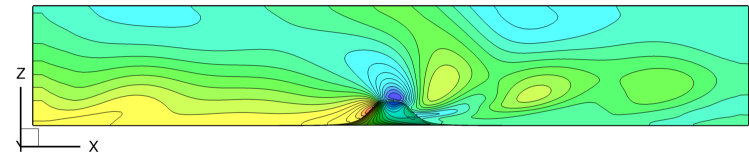
truncated domain +H



truncated domain +H

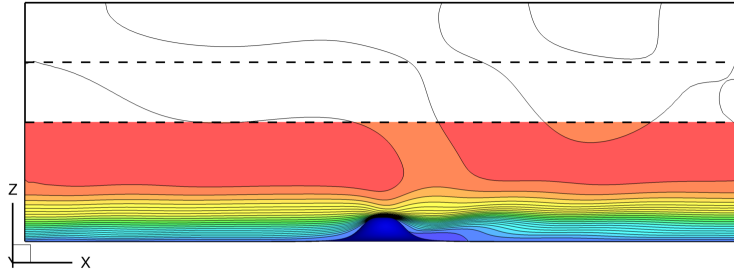


truncated domain
 $\frac{\partial p}{\partial n} = 0$

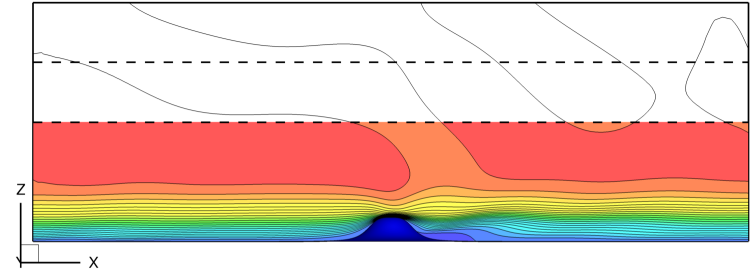


truncated domain
CPD

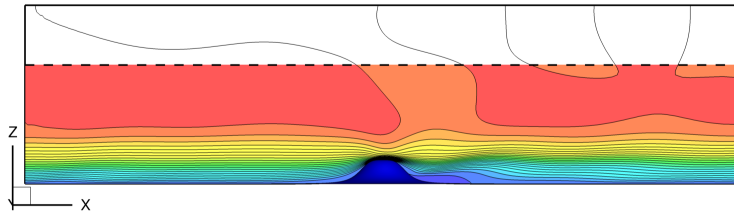
Longitudinal velocity contours in the plane of symmetry.



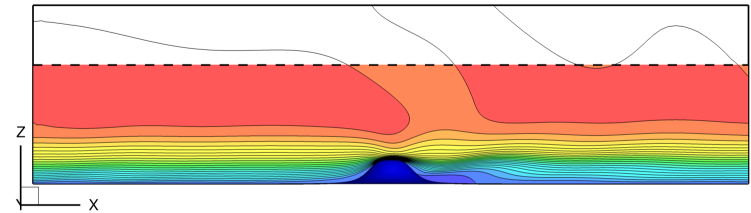
truncated domain $+2H$



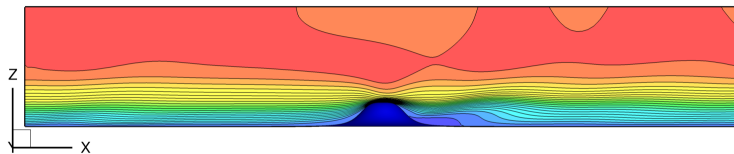
truncated domain $+2H$



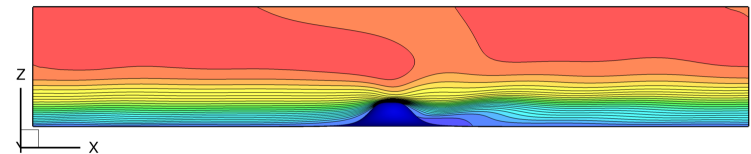
truncated domain $+H$



truncated domain $+H$

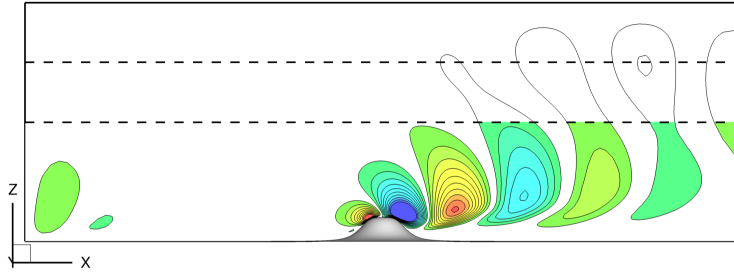


*truncated domain
 $\frac{\partial p}{\partial n} = 0$*

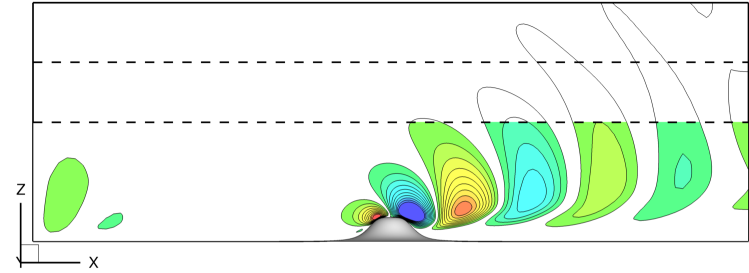


*truncated domain
CPD*

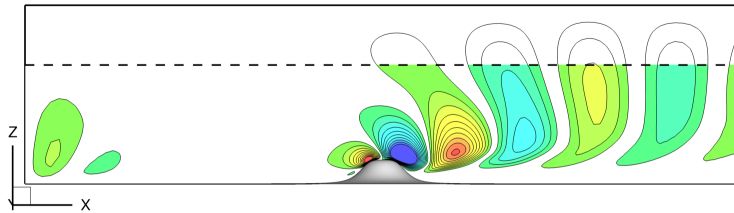
Vertical velocity contours in the plane of symmetry.



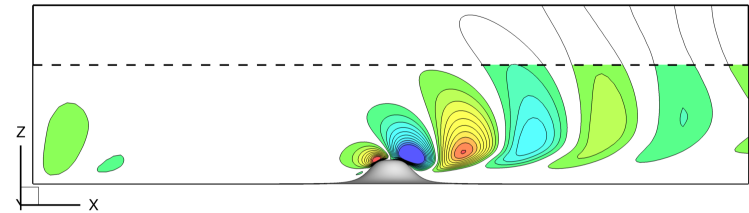
truncated domain +2H



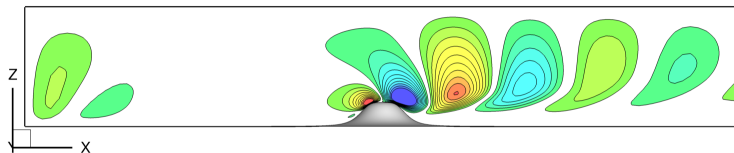
truncated domain +2H



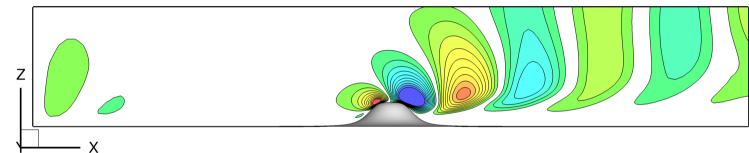
truncated domain +H



truncated domain +H



truncated domain
 $\frac{\partial p}{\partial n} = 0$



truncated domain
CPD

8. Conclusions & Remarks

- *Physical interpretation/justification of the CPD condition*

$$\frac{\partial p}{\partial n} = \rho^* |\mathbf{u}| \frac{\partial u_n}{\partial n}$$

The term $\frac{\partial u_n}{\partial n}$ is really essential. It can be better understood when a local coordinate system is adopted at an artificial boundary point. Let us, e.g., assume that the (outer) normal direction is associated with the z axis, while the x and y axes now define a tangential plane (to boundary). Due to the divergence-free constraint $u_x + v_y + w_z = 0$, the value of normal derivative of normal velocity component w_z indicates to what extent the tangential, two-dimensional continuity equation $u_x + v_y = 0$ is satisfied, i.e. $u_x + v_y = -w_z$. So, when $w_z = 0$, the flow field can be seen as locally two-dimensional and it makes a sense to drop the pressure derivative in the third (normal) direction.

In the absence (or negligibility) of local viscous forces, the pressure gradient should compensate the inertia represented by the convective term. Thus the proportionality factor (with respect the normal velocity normal derivative $\frac{\partial u_n}{\partial n} = w_z$) was set to $\rho^* |\mathbf{u}|$, which assures the proper (convective term like) scaling and is invariant to the orientation of the chosen coordinate system.

- *No-slip wall & Inlet* – It is good to note that at the no-slip wall (where $|\mathbf{u}| = 0$) the CPD condition reduces to the classical homogeneous Neumann pressure condition. Also at the inlet, where $\frac{\partial u_n}{\partial n}$ vanishes (e.g., due to prescribed $u_\tau = 0$) the homogeneous Neumann condition for pressure is recovered. So, in fact, we can claim, that in our case we have used the CPD condition on all boundaries, except the outlet.
- *Velocity at the far-field boundaries* – The (linear) extrapolation (equivalent to the use of one-sided (backward) first order approximation of derivatives at the boundary points) of all velocity components used in this study seems to work well for the solved test case. The possibility of using the homogeneous Neumann condition for the tangential components of velocity (while keeping the extrapolation for the normal one), was successfully tested. It has only marginal (but yet visible) effect on the solution close to the boundary. Its use however can be of some importance in the theoretical analysis of the model.

THE END

References

- [1] BODNÁR, T. & BENEŠ, L.: On Some High Resolution Schemes for Stably Stratified Fluid Flows. In: *Finite Volumes for Complex Applications VI, Problems & Perspectives*, vol. 4 of *Springer Proceedings in Mathematics*, (pp. 145–153). Springer Verlag (2011).
- [2] BODNÁR, T., BENEŠ, L., FRAUNIÉ, P., & KOZEL, K.: Application of compact finite-difference schemes to simulations of stably stratified fluid flows. *Applied Mathematics and Computation*, vol. 219, no. 7: (2012) pp. 3336–3353.
- [3] BODNÁR, T., FRAUNIÉ, P., KNOBLOCH, P., & ŘEZNÍČEK, H.: Numerical Evaluation of Artificial Boundary Condition for Wall Bounded Stably Stratified Flows. *Discrete and Continuous Dynamical Systems. Series S*, vol. 14, no. 3: (2021) pp. 785–801.
- [4] BODNÁR, T., FRAUNIÉ, P., & ŘEZNÍČEK, H.: Numerical Tests of Far-Field Boundary Conditions for Stably Stratified Stratified Flows. In: *Topical Problems of Fluid Mechanics 2019*, (pp. 1–8). Institute of Thermomechanics CAS, Prague (2019).
- [5] BRAACK, M. & MUCHA, P.: Directional Do-Nothing Condition for the Navier-Stokes Equations. *Journal of Computational Mathematics*, vol. 32, no. 5: (2014) pp. 507–521.
- [6] CHASHECHKIN, Y. & MITKIN, V.: A visual study on flow pattern around the strip moving uniformly in a continuously stratified fluid. *Journal of Visualization*, vol. 7, no. 2: (2004) pp. 127–134.
- [7] CHASHECHKIN, Y., MITKIN, V., & BARDAKOV, R.: Streaky structures in the stratified flow over a horizontal strip. *Doklady Physics*, vol. 51, no. 8: (2006) pp. 454–458.
- [8] DING, L., CALHOUN, R. J., & STREET, R. L.: Numerical Simulation of Strongly Stratified Flow Over a Three-Dimensional Hill. *Boundary-Layer Meteorology*, vol. 107, no. 1: (2003) pp. 81–114.
- [9] GAITONDE, D. V., SHANG, J. S., & YOUNG, J. L.: Practical aspects of higher-order numerical schemes for wave propagation phenomena. *International Journal for Numerical Methods in Engineering*, vol. 45: (1999) pp. 1849–1869.
- [10] GOTTLIEB, S.: On High Order Strong Stability Preserving Runge-Kutta and Multi Step Time Discretizations. *Journal of Scientific Computing*, vol. 25, no. 1: (2005) pp. 105–128.
- [11] GOTTLIEB, S. & SHU, C. W.: Total Variation Diminishing Runge-Kutta Schemes. *Mathematics of Computation*, vol. 67, no. 221: (1998) pp. 73–85.

- [12] GOTTLIEB, S., SHU, C. W., & TADMOR, E.: Strong Stability-Preserving High-Order Time Discretization Methods. *SIAM Review*, vol. 43, no. 1: (2001) pp. 89–112.
- [13] HEYWOOD, J., RANNACHER, R., & TUREK, S.: Artificial boundaries and flux and pressure conditions for the incompressible Navier-Stokes equations. *International Journal for Numerical Methods in Fluids*, vol. 22: (1996) pp. 325–352.
- [14] HUNT, J. C. R. & SNYDER, W. H.: Experiments on stably and neutrally stratified flow over a model three-dimensional hill. *Journal of Fluid Mechanics*, vol. 96, no. 4: (1980) pp. 671–704.
- [15] LELE, S. K.: Compact Finite Difference Schemes with Spectral-like Resolution. *Journal of Computational Physics*, vol. 103: (1992) pp. 16–42.
- [16] LIONS, P.: *Mathematical Topics in Fluid Mechanics, Volume I – Incompressible Models*, vol. 3 of *Oxford Lecture Series in Mathematics and Its Applications*. Oxford Univeristy Press (1996).
- [17] SHU, C. W.: Total-Variation-Diminishing time discretizations. *SIAM Journal of Scientific & Statistical and Computing*, vol. 9: (1988) pp. 1073–1084.
- [18] SHU, C. W. & OSHER, S.: Efficient implementation of essentially non-oscillatory shock-capturing schemes. *Journal of Computational Physics*, vol. 77: (1988) pp. 439–471.
- [19] SPITERI, R. J. & RUUTH, S. J.: A new class of optimal high-order strong-stability-preserving time discretization methods. *SIAM Journal on Numerical Analysis*, vol. 40, no. 2: (2002) pp. 469–491.
- [20] VISBAL, M. & GAITONDE, D.: On the Use of Higher-Order Finite-Difference Schemes on Curvilinear and Deforming Meshes. *Journal of Computational Physics*, vol. 181: (2002) pp. 155–185.